11

Harmonic Distortion in Renewable Energy Systems: Capacitive Couplings

Miguel García-Gracia, Nabil El Halabi,
Adrián Alonso and M.Paz Comech
CIRCE (Centre of Research for Energy Resources and Consumption)
University of Zaragoza
Spain

1. Introduction

Renewable energy systems such as wind farms and solar photovoltaic (PV) installations are being considered as a promising generation sources to cover the continuous augment demand of energy.

With the incoming high penetration of distributed generation (DG), both electric utilities and end users of electric power are becoming increasingly concerned about the quality of electric network (Dugan et al., 2002). This latter issue is an umbrella concept for a multitude of individual types of power system disturbances. A particular issue that falls under this umbrella is the capacitive coupling with grounding systems, which become significant because of the high-frequency current imposed by power converters.

The major reasons for being concerned about capacitive couplings are:

a. Increase the harmonics and, thus, power (converters) losses in both utility and customer equipment.
b. Ground capacitive currents may cause malfunctioning of sensitive load and control devices.
c. The circulation of capacitive currents through power equipments can provoke a reduction of their lifetime and limits the power capability.
d. Ground potential rise due to capacitive ground currents can represent unsafe conditions for working along the installation or electric network.
e. Electromagnetic interference in communication systems and metering infrastructure.

For these reasons, it has been noticed the importance of modelling renewable energy installations considering capacitive coupling with the grounding system and thereby accurately simulate the DC and AC components of the current waveform measured in the electric network.

Introducing DG systems in modern distribution networks may magnify the problem of ground capacitive couplings. This is because DG is interfaced with the electric network via power electronic devices such as inverters.

These capacitive couplings are part of the electric circuit consisting of the wind generator, PV arrays, AC filter elements and the grid impedance, and its effect is being appreciated in most large scale DG plants along the electric network (García-Gracia et al., 2010).

Power electronic devices, as used for DG, might be able to cause harmonics. The magnitude and the order of harmonic currents injected by DC/AC converters depend on the technology of the converter and mode of its operation (IEC Std. 61000-4-7, 2010, IEEE Std. 519-1992, 1992). Due to capacitive coupling between the installation and earth, potential differences imposed by switching actions of the converter inject a capacitive ground current which can cause significant electromagnetic interferences, grid current distortion, losses in the system, high-noise level in the installation and unsafe work conditions (Chicco et al., 2009).
Several renewable system installations analyses have been reported (Bellini, 2009, Conroy, 2009, Luna, 2011, Sukamonkol, 2002, Villalva, 2009), where most theoretical analysis and experimental verifications have been performed for small-scale installations without considering capacitive coupling. Power electronics models and topologies also have been studied, but without considering the amount of losses produced by the capacitive current that appears due to the switching actions (Zhow, 2010, Chayawatto, 2009, Kim, 2009). In (Iliceto & Vigotti, 1998), the total conversion losses of a real 3 MW PV installation have been studied considering reflection losses, low radiation and shadow losses, temperature losses, auxiliary losses, array losses and converters losses. The latter two factors sum a total of 10% of the rated power where part of these losses is due to the capacitive coupling that was neglected.
Therefore, for an accurate study of power quality, it is important to model DG installations detailing the capacitive coupling of the electric circuit with the grounding system, which are detailed for PV installations and wind farms in Sections 2 and 3, respectively. These models allow analyzing the current distortion, ground losses and Ground Potential Rise (GPR) due to the capacitive coupling. The combined effect of several distributed generation sources connected to the same electric network has been simulated, and results have been presented together with solutions based on the proposed model to minimize the capacitive ground current for meeting typical power quality regulations concerning to the harmonic distortion and safety conditions.

2. Capacitive coupling in solar-photovoltaic installation

The region between PV modules and PV structure essentially acts as an insulator between layers of PV charge and ground. Most shunt capacitive effects that may be ignored at very low frequencies can not be neglected at high frequencies for which the reactance will become relatively small due to the inverse proportionality with frequency *f* and, therefore, a low impedance path is introduced between power elements and ground.
This effect is present in PV installations because of the high frequency switching carried out by the converters stage, which arises different capacitive coupling between modules and ground. Thus, the capacitive effect must be represented as a leakage loop between PV arrays, cables and electronic devices and the grounding system. By means of this leakage loop, capacitive currents are injected into the grounding system creating a GPR along the PV installation which introduces current distortion, electromagnetic interference, noise and unsafe work conditions. For this reason, an accurate model of these capacitive couplings are requiered for PV installations.

2.1 Equivalent electric circuit for ground current analysis

Depending on the switching frequency, the harmonics produced may be significant according to the capacitive coupling and the resonant frequency inside the PV installation.

Moreover, every PV array is considered as an independent current source with a DC current ripple independent of the converter ripple. These ripple currents are not in synchronism with the converter and produce subharmonics in the DC circuit which increase the Total Harmonic Distortion in the current waveform (THDI) (Zhow et al., 2010).
The typical maximum harmonic order h = 40, defined in the power quality standards, corresponds to a maximum frequency of 2 kHz (with 50 Hz as fundamental frequency) (IEC Std. 61000-4-7, 2002). However, the typical switching frequency of DC/DC and DC/AC converters, usually operated with the Pulse Width Modulation (PWM) technique, is higher than 3 kHz. Hence, higher order harmonics up to the 100th order, can be an important concern in large scale PV installations where converters with voltage notching, high pulse numbers, or PWM controls result in induced noise interference, current distortion, and local GPR at PV arrays (Chicco et al., 2009).
A suitable model of capacitive couplings allows reproducing these harmonic currents injected not only into the grid, but also into the DC circuit of the PV installation that would lead to internal resonant, current distortion and unsafe work conditions where capacitive discharge currents could exceed the threshold of safety values of work (IEEE Std. 80-2000, 2000). The capacitive coupling is part of the electric circuit consisting of the PV cells, cables capacitive couplings, AC filter elements and the grid impedance, as shown in Fig. 1, and its effect is being appreciated in most large scale PV plants.

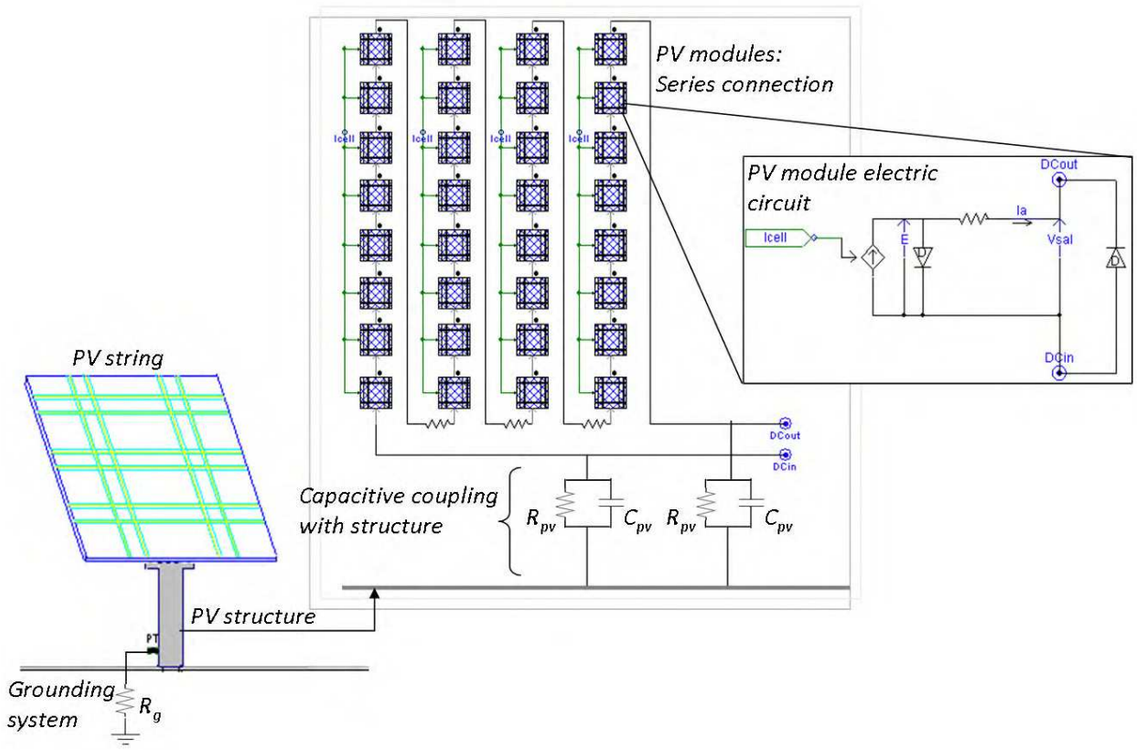

Fig. 1. Model of PV module, PV array and capacitive coupling with PV structure.

2.2 Behavior of the PV installation considering capacitive coupling

Normally, numerous PV modules are connected in series on a panel to form a PV array as it is shown in Fig. 1. The circuit model of the PV module (Kim et al., 2009) is composed of an ideal current source, a diode connected in parallel with the current source and a series resistor. The output current of each PV module is determined as follows:

$$I = I_{sc} - I_d = I_{sc} - I_o \cdot \left[\exp\left(\frac{V + I \cdot R_s}{n \cdot V_T} \right) \right] \tag{1}$$

where I_o is the diode saturation current, V the terminal voltage of a module, n the ideal constant of diode, V_T is the thermal potential of a module and it is given by $m \cdot (kT/q)$ where k the Boltzmann's constant (1.38E-23 J/K), T the cell temperature measured in K, q the Coulomb constant (1.6E-19 C), and m the number of cells in series in a module. I_{sc} is the short circuit current of a module under a given solar irradiance. I_d is the diode current, which can be given by the classical diode current expression. The series resistance R_s represents the intrinsic resistance to the current flow.

The capacitive coupling of PV modules with the ground is modelled as a parallel resistance R_{pv} and capacitor C_{pv} arrangement which simulates the frequency dependency on the insulator between PV modules and the grounding system. The PV structure is connected to the grounding system represented in the model by the grounding resistance R_g.

Taking into account that the converter represents a current source for both DC circuit and AC circuit of the PV installation, an equivalent circuit is deduced to analyze the capacitive coupling effect over the current and voltage waveforms.

The equivalent circuit of both DC circuit of the PV installation and AC circuit for connection to the grid as seen between inverter terminals and ground is illustrated Fig. 2. In the AC circuit R_{ac_cable}, L_{ac_cable} and C_{ac_cable} are the resistance, inductance and capacitance of the AC underground cables, R_{g_es} is the ground resistance at the substation and L_{filter} and C_{filter} are the parameters of the LC filter connected at AC terminals of the inverter.

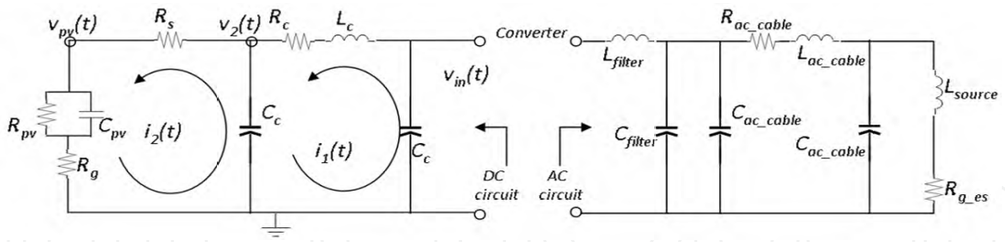

Fig. 2. Capacitive coupling model for the DC and AC electric circuit of a PV installation.

The inclusion of R_{pv} and C_{pv} on the PV equivalent circuit allows representing the leakage path for high frequency components between PV modules and ground. This DC equivalent circuit is represented by the following continuous-time equations, at nominal operating condition

$$\frac{di_1(t)}{dt} = \frac{1}{L_c} \cdot v_{in}(t) - \frac{R_c}{L_c} \cdot i_1(t) - \frac{1}{L_c} \cdot v_2(t) \tag{2}$$

$$\frac{di_2(t)}{dt} = \frac{1}{C_c \cdot (R_s + R_g)} \cdot i_1(t) - \left[\frac{1}{C_c \cdot (R_s + R_g)} + \frac{\psi}{C_{pv} \cdot R_{pv}} \right] \cdot i_2(t) + \frac{1}{C_{pv} \cdot R_{pv} \cdot (R_s + R_g)} \cdot v_2(t) \tag{3}$$

$$\frac{dv_2(t)}{dt} = \frac{1}{C_c}\cdot i_1(t) - \frac{1}{C_c}\cdot i_2(t) \tag{4}$$

$$\frac{dv_{pv}(t)}{dt} = \frac{R_g}{C_c\cdot(R_s+R_g)}\cdot i_1(t) + \left(\frac{R_{pv}+R_g}{C_{pv}\cdot R_{pv}} - \frac{R_g}{C_c\cdot(R_s+R_g)} - \frac{R_g\cdot\psi}{C_{pv}\cdot R_{pv}}\right)\cdot i_2(t)\ldots + \frac{R_g}{C_{pv}\cdot R_{pv}\cdot(R_s+R_g)}\cdot v_2(t) - \frac{1}{C_{pv}\cdot R_{pv}}\cdot v_{pv}(t) \tag{5}$$

According to the equivalent DC circuit shown in Fig. 2, $i_1(t)$ and $i_2(t)$ are the current of mesh 1 and mesh 2, respectively, $v_{in}(t)$ is the injected voltage by the converter, $v_2(t)$ the voltage at node 2 and $v_{pv}(t)$ is the voltage between PV module and ground and represents the parameter under study. Parameter C_c represents the capacitive coupling between cables and ground and R_c and L_c are the resistance and inductance of the cable, respectively.

In some simplified models of PV installation (Villalva, 2009, Kim, 2009, Bellini, 2009), the capacitance C_{pv} and resistance R_{pv} are considered like infinite and zero, respectively. Then, the capacitive coupling with the grounding system is totally neglected. Even ground resistance of the PV installation is not considered ($R_g = 0$).

The PV arrays are connected to a DC system of 700 V, and the power is delivered to an inverter stage based on four inverters of 125 kW in full bridge topology and operation frequency of 3.70 kHz. The underground cables, which connect the PV arrays to the inverter stage, have been included through their frequency dependent model.

The electrical parameters of the capacitive coupling between PV arrays and grounding system are shown in Table 1 and have been adjusted according to the field measurement in order to simulate the response of the capacitive coupling model accurately against the harmonics injected by the operation of the converters.

Element	Parameter	Value
PV array	Operation voltage	700 Vdc
	Capacitance C_{PV}	$1x10^{-9}$ F
	Resistance R_{PV}	$1x10^{7}$ Ω
	Series Resistance R_S	0.30 Ω
DC cable	Resistance R_C	0.25 Ω/km
	Inductance L_C	0.00015 H/km
	Capacitive coupling C_C	$1x10^{-4}$ F/km
Filter LC	Inductance L_{filter}	90 μH
	Capacitance C_{filter}	0.756 mF
Underground cable	Positive sequence impedance	0.3027 + *j* 0.1689 Ω/km
	Zero sequence impedance	0.4503 + *j* 0.019 Ω/km
	Zero sequence susceptance	0.1596 mS/km
Power grid	Thevenin voltage	20 kV
	Thevenin impedance	0.6018+*j* 2.4156 Ω
	Ground resistance R_g	1.2 Ω

Table 1. Electric parameters for the solar PV installation capacitive grounding model.

The frequency response of both capacitive coupling and simplified model for the DC circuit of a PV installation operating at nominal operating condition is shown in the Bode diagram of Fig. 3. The capacitive coupling model presents a considerable gain for waveforms under 108 kHz in comparison with the simplified model which has a limited gain for this range of frequencies. Hence, the capacitive coupling model is able to simulate the leakage loop between PV module and grounding system for high frequencies, unlike the simplified model.

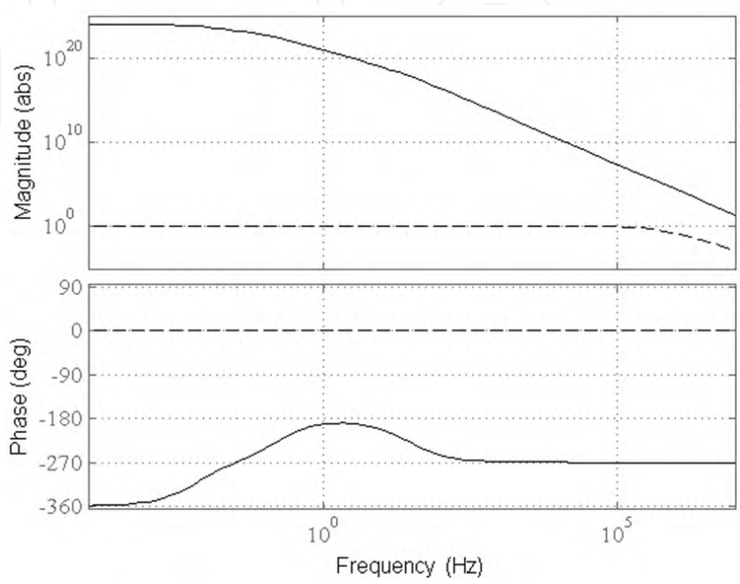

Fig. 3. Bode diagram for both capacitive coupling model (solid line) and simplified model (dashed line) for the DC circuit of a PV installation.

The PV installation modelled consists of 184 PV arrays connected in parallel to generate 1 MW. Both circuits have been modelled to analyze the mutual effect raised from the capacitive couplings between the electric circuits and the grounding system, at rated operating conditions. The simulation has been performed using PSCAD/EMTDC [PSCAD, 2006] with a sampling time of at least 20 μs.

The current and voltage waveforms obtained from the proposed model together with the FFT analysis are shown in Fig. 4a and Fig. 4b. The THDI and THDV obtained from simulations are 26.99% and 3725.17%, respectively, where the DC fundamental component of current is 88.56 mA, and the fundamental voltage component is 8.59 V. The frequencies where most considerable harmonic magnitudes are the same of those obtained at field measurement; 3.70 kHz, 11.10 kHz, 14.80 kHz and 18.50 kHz within a percentage error of ±27.42% for fundamental component and ±15.35% for the rest of harmonic components.

2.3 Additional information provided by the PV installation capacitive coupling

The model considering capacitive coupling between PV modules and grounding system of the installation leads to an accurate approximation to the response of the PV installation against the frequency spectrum imposed by the switching action of the inverters. This approximation is not feasible using simplified models because of the bandwidth limitation shown in Fig. 3 for high frequencies.

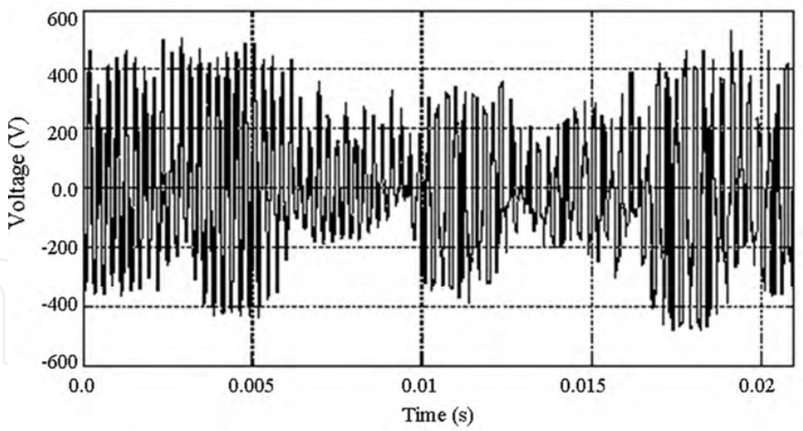

(a)

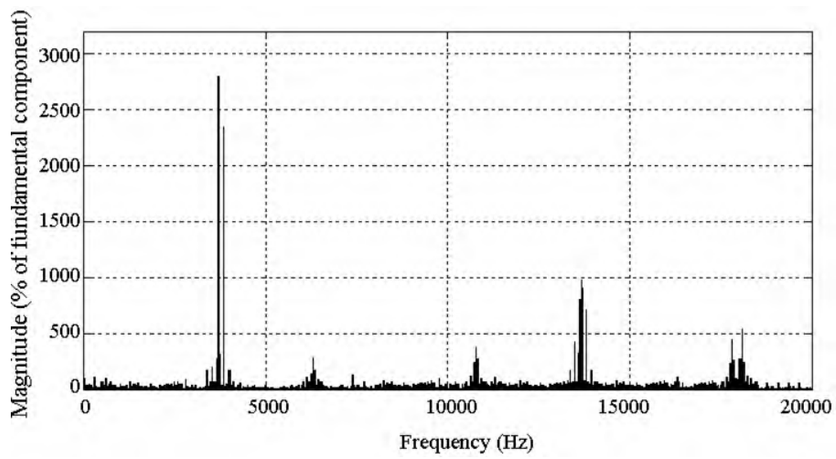

(b)

Fig. 4. Simulation result of the capacitive coupling model: (a) voltage waveform between PV array and grounding system and (b) FFT analysis of the voltage waveform obtained.

Simulation results indicate that ground current in large scale PV installations can be considerable according to the values expressed in (IEEE Std. 80-2000, 2000). In the range of 9-25 mA range, currents may be painful at 50-60 Hz, but at 3-10 kHz are negligible (IEC 60479-2, 1987). Thus, the model allows the detection of capacitive discharge currents that exceeds the threshold of safety values at work.

Because of large scale installations are systems with long cables, the resonant frequency becomes an important factor to consider when designing the AC filters and converters operation frequency. The proposed model accurately detects the expected resonant frequency of the PV installations at 12.0 kHz with an impedance magnitude Z of 323.33 Ω while simplified models determine a less severe resonant at a frequency value of 15.50 kHz with a Z of 150.45 Ω, as shown in Fig. 5.

This latter resonant frequency is misleading and pointless for the real operating parameters of the installation. The total DC/AC conversion losses obtained from simulations is 5.6% when operating at rated power, which is equivalent to 56.00 kW. Through the proposed model, it has been detected that a 22.32% of the losses due to the DC/AC conversion is

because of the capacitive coupling modelled. Thus, a 1 MW PV installation as modelled in Fig. 2 presents 12.50 kW of losses due to the capacitive couplings or leakage loop between PV modules and ground.

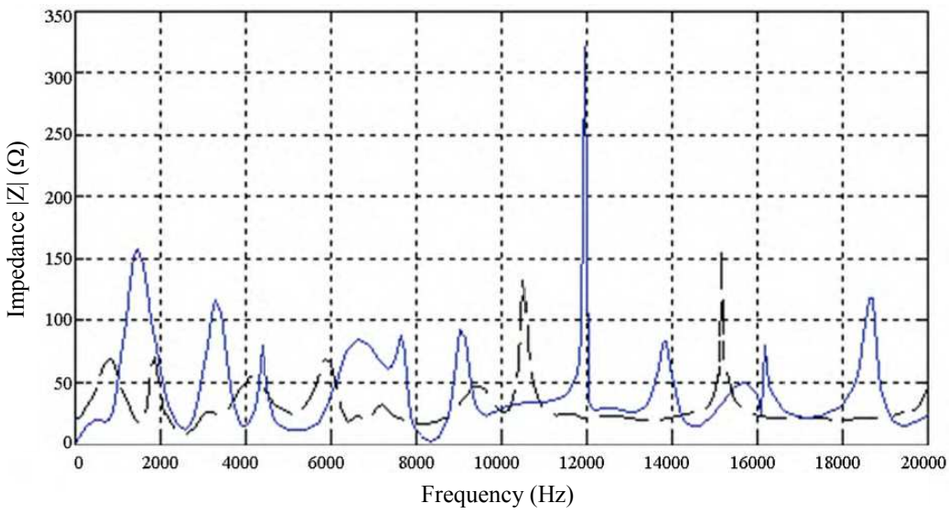

Fig. 5. Resonance frequency of the PV installation without capacitive coupling (dashed line) and considering capacitive couplings (solid line).

3. Capacitive coupling in wind farms

Wind energy systems may contribute to the distribution network voltage distortion because of its rotating machine characteristics and the design of its power electronic interface. As presented in Fig. 6, wind energy system designs incorporate a wide range of power electronic interfaces with different ratings (Comech et al., 2010).

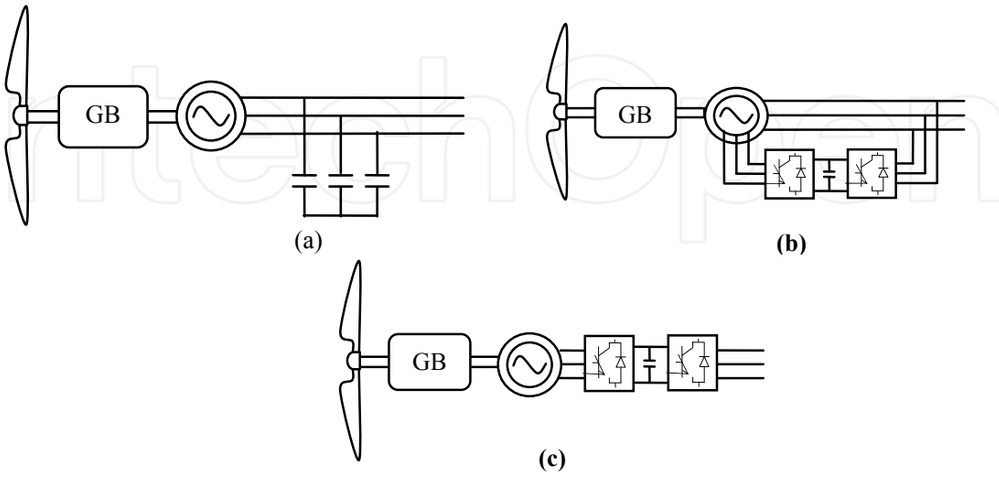

Fig. 6. Wind turbine configurations.

Fig. 6a shows the fixed-speed wind turbine with asynchronous squirrel cage induction generator (SCIG) directly connected to the grid via transformer. Fig. 6b represents the limited variable speed wind turbine with a wound rotor induction generator and partial scale frequency converter on the rotor circuit known as doubly fed induction generator (DFIG). Fig. 6c shows the full variable speed wind turbine, with the generator connected to the grid through a full-scale frequency converter.

These power electronic interfaces are rated as a percentage of the machine power, hence larger systems are accountable for higher distortions. Recent investigations based on wind energy systems suggests that frequency converters (with a typical pulse width modulated with 2.5 kHz of switching frequency) can, in fact, cause harmonics in the line current, leading to harmonic voltages in the network (Conroy & Watson, 2009).

Moreover, most simplified models of wind farms consider a simple series impedance model for underground cables that connect wind turbines with the network grid. Thus, capacitive couplings with ground through cables are not considered for different frequencies components.

To simulate wind farms harmonic distortion behaviour accurately, it is important to model cables by their frequency dependent model. The equivalent circuit for the capacitive coupling model of wind farms is shown in Fig. 7.

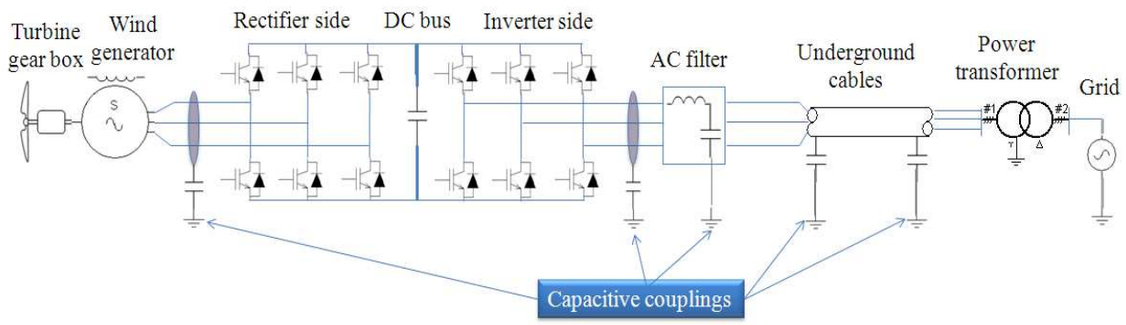

Fig. 7. Capacitive coupling model for wind farm.

Notice that, otherwise the capacitive model of solar installations, the wind turbine is directly connected to the rectifier side of the converter. The capacitive coupling seen by the DC bus through the wind turbine is composed of the path between the rectifier side and ground because of the high harmonic current component imposed by the switching actions, whereas the capacitive coupling seen through the grid is represented by the inverter side, the filter and the underground cable. The equivalent electric circuit of the wind farm capacitive coupling model is shown in Fig. 8.

In this figure, parameters R_{WG} and L_{WG} make reference to the resistance and inductance, respectively, of the synchronous wind generator. R_g is the ground resistance at the wind turbine location while R_{q_es} is the ground resistance of the electrical substation belonging to the wind farm under study.

$C_{rectifier}$ and C_{ac_cable} are the capacitive couplings of the rectifier side and underground cable, respectively, with ground. R_{ac_cable} and L_{ac_cable} make reference to the resistance and inductance, respectively, of the synchronous wind generator. L_{filter} and C_{filter} are the dimensions of the filter. L_{TR} is the equivalent impedance of the power transformer and L_{source} the thevenin impedance of the source. The variables $v_{WT}(t)$ and $v_{source}(t)$ are the voltages at wind generator node and network grid source, respectively. The input voltage $v_{in}(t)$ is the voltage injected into the grid by the inverter side.

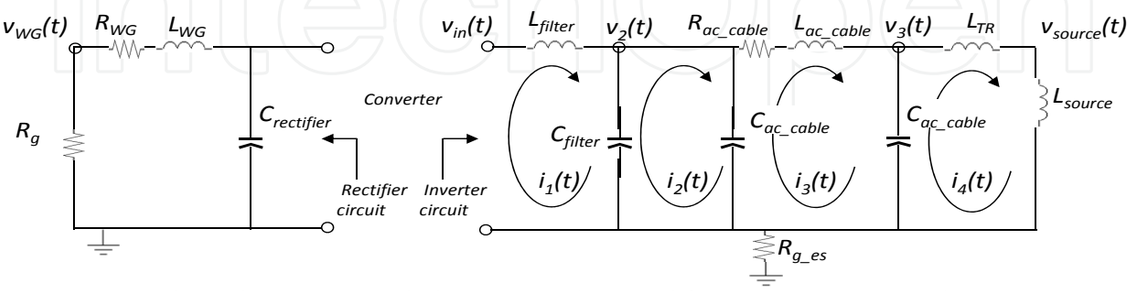

Fig. 8. Equivalent electric circuit belonging to the wind farm capacitive coupling.

The state variable representing this model can be deduced in a similar way as expressed in Section 2. Nonetheless, the effect of capacitive couplings in wind farms is more significant at the inverter circuit through the power grid where the circuit of the filters and cables exert an important influence over the ground currents.

The continuous time equations that describe the transfer function between the input voltage $v_{in}(t)$ and the network grid $v_{source}(t)$ are the following

$$\frac{di_1(t)}{dt} = \frac{1}{L_{filter}} \cdot \left(v_{in}(t) - v_2(t)\right) \tag{6}$$

$$\frac{dv_2(t)}{dt} = \frac{1}{\left(C_{filter} + C_{ac\_cable}\right)} \cdot \left(i_1(t) - i_3(t)\right) \tag{7}$$

$$\frac{di_3(t)}{dt} = \frac{1}{L_{fac\_cable}} \cdot \left(v_2(t) - i_3(t) \cdot R_{ac\_cable} - v_3(t)\right) \tag{8}$$

$$\frac{dv_3(t)}{dt} = \frac{i_3(t) - i_4(t)}{C_{ac\_cable}} \tag{9}$$

$$\frac{di_4(t)}{dt} = \frac{v_3(t)}{L_{TR} + L_{source}} \tag{10}$$

The electric parameters related to the capacitive coupling model of Fig. 8 are shown in Table 2. In Fig. 9a, the ground voltage measurement is shown while in Fig. 9b the FFT analysis for this waveform is shown. It is observed that the harmonics components near the switching frequency are considerably higher than the fundamental component. Harmonics components 70 (3500 Hz) is 575% of fundament component magnitude which is 3.05 V. That means that

harmonic 70 has a magnitude of 17.54 V, as shown in Fig. 9a. Moreover, the multiples of the switching frequencies are also considerable respect to the fundamental component, as shown in Fig. 9b, where the harmonic component 138 (7000 Hz) and 210 (10500 Hz) are approximately 145% and 98%, respectively, of the fundamental component magnitude.
The ground current waveform measured at the wind farm is shown in Fig. 10a, and the FFT analysis concerning this waveform is performed in Fig. 10b. Consistently with the voltage waveform, the dominant harmonic component in the ground current fits the switching frequency of the converter. That is harmonic component 68 with 503% of the fundamental component magnitude which is 168 mA. Thus, the magnitude of harmonic 68 is 844.9 mA.

Element	Parameter	Value
Wind generator	Operation voltage	3.5 kV
	Operation frequency	50 Hz
	Nominal power	1400 kVA
	Stator winding resistance	0.01196 pu
	Stator leakage reactance	0.1966 pu
Full converter	Nominal power	1800 kVA
	Switching frequency	3500 Hz
	Topology	6 pulses
	Capacitive coupling	0.8 uF
Filter	Q factor	10
	Cut-off frequency	1000 Hz
	Nominal power	530 kVA
Underground cable	Positive sequence impedance	0.09015+*j* 0.0426 Ω/km
	Zero sequence impedance	0.0914 + *j* 0.03446 Ω/km
	Zero sequence susceptance	0.327 mS/km
Power grid	Thevenin voltage	3.5 kV
	Thevenin inductance	0. 231 mH

Table 2. Electric parameters for the wind farm capacitive grounding model.

The multiples of the switching frequencies are also significant, as shown in Fig. 10b, however harmonic component 140 (7000 Hz) appears higher than in the ground voltage waveform near to 200% while harmonic 210 (10500 Hz) is less dominant, 56% but still high enough in comparison with the fundamental component.
These simulation results indicate that ground current in wind farms can be considerable according to the values expressed in (IEEE 80-2000, 2000) for the range of frequencies expressed at Fig. 10a. Therefore, care is then needed to ensure that ground current is within safe limits of work.
This issue is one of the most significant advantages of considering capacitive coupling models for wind farms, which allows implementing further corrective actions to mitigate the adverse effect of ground current over safe conditions of work.
The capacitive coupling model detects the expected resonant frequency of the wind farm at 11.0 kHz with an impedance magnitude Z of 77.8 Ω while simplified models does not detect a resonant frequency for this wind farm configuration, as shown in Fig. 11.

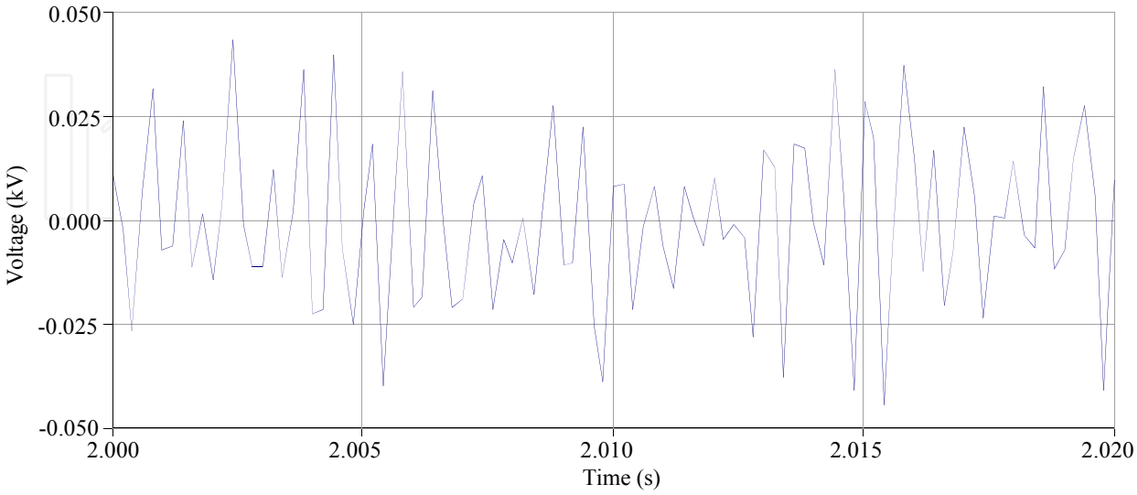

(a)

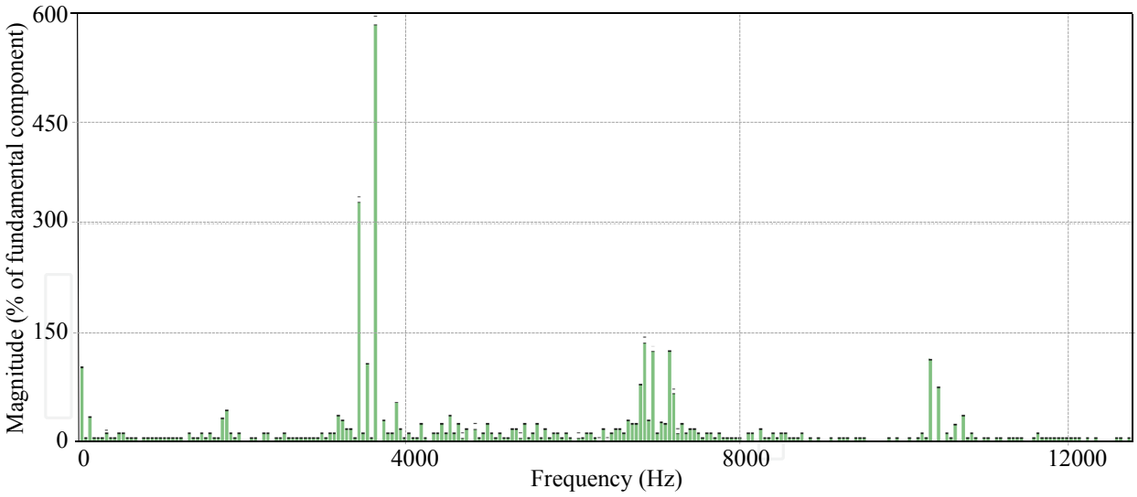

(b)

Fig. 9. Simulation result of the capacitive coupling model: (a) voltage waveform between wind farm electric circuit and grounding system and (b) FFT analysis of the voltage waveform obtained.

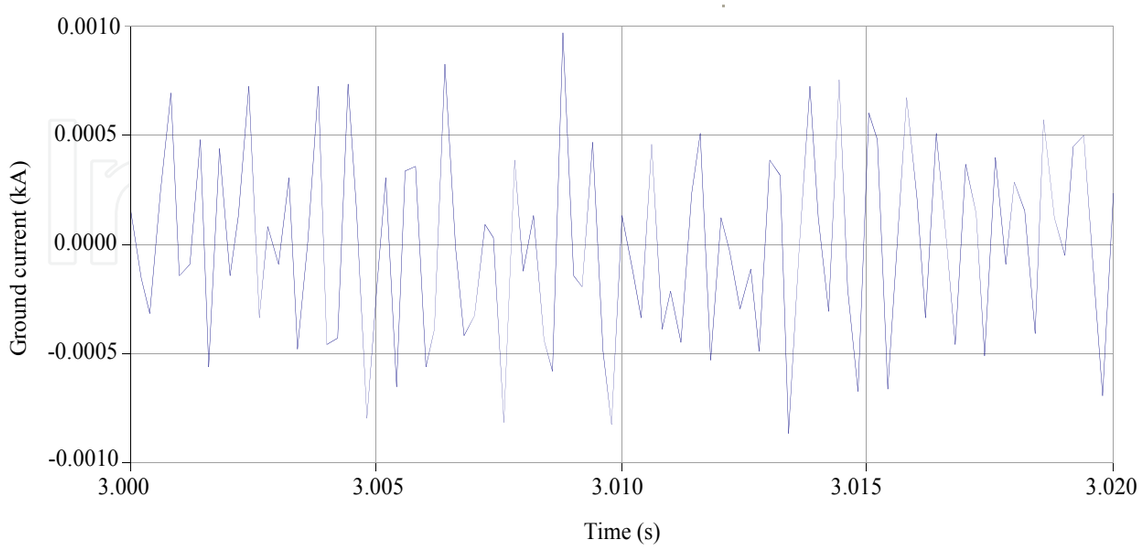

(a)

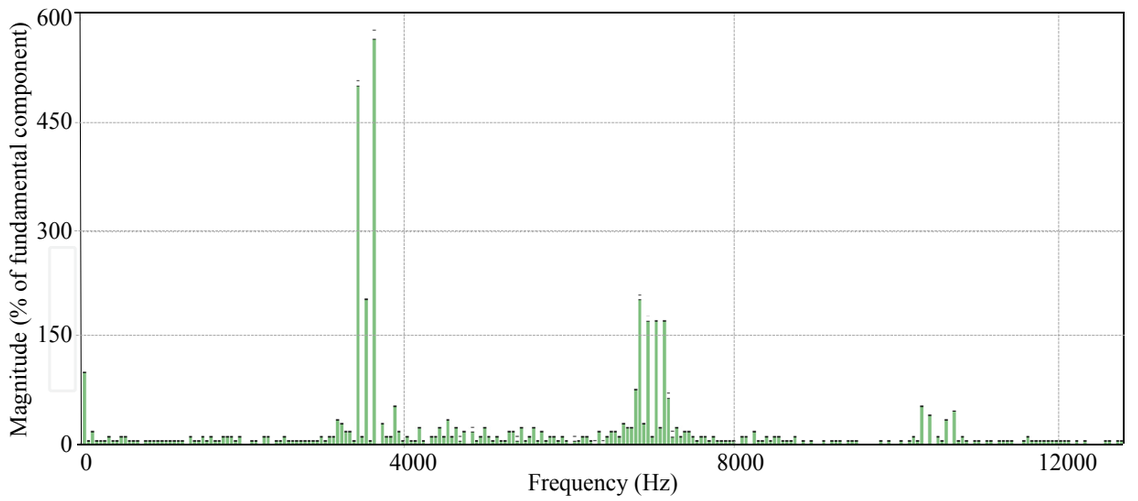

(b)

Fig. 10. Simulation result of the capacitive coupling model: (a) waveform between wind farm electric circuit and ground and (b) FFT analysis of the ground current obtained.

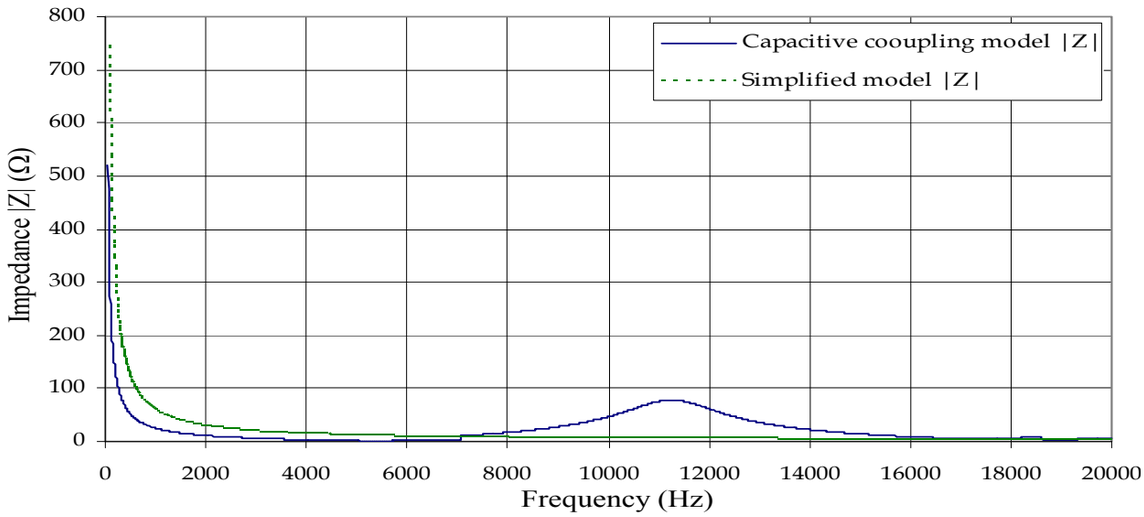

Fig. 11. Resonance frequency of the wind farm model without considering capacitive coupling (dashed line) and with capacitive couplings (solid line).

4. Impact on distribution networks of DG ground current contribution

The distribution network considering DG, shown in Fig. 12, has been modelled to analyze the effects of wind farms and PV solar installations ground current contribution to the network. The DG is based on capacitive coupling models of a 1 MW PV solar installation and a 1.4 MW wind farm with the electric parameters shown in Table 1 and Table 2, respectively.

This distribution network feeds two loads through a multi-terminal ring topology. These loads are connected to bus 2 and 5 with a rated power of 500+ *j* 25 kVA each one.

In steady state conditions, the wind farm generates a total active power of 1370 kW, and the PV solar installation delivered 940 kW to the distribution network. To analyse the capacitive coupling effect over the ground current in DG systems, it has been noticed the voltage and current waveforms seen at node 5 through the capacitive coupling of the line.

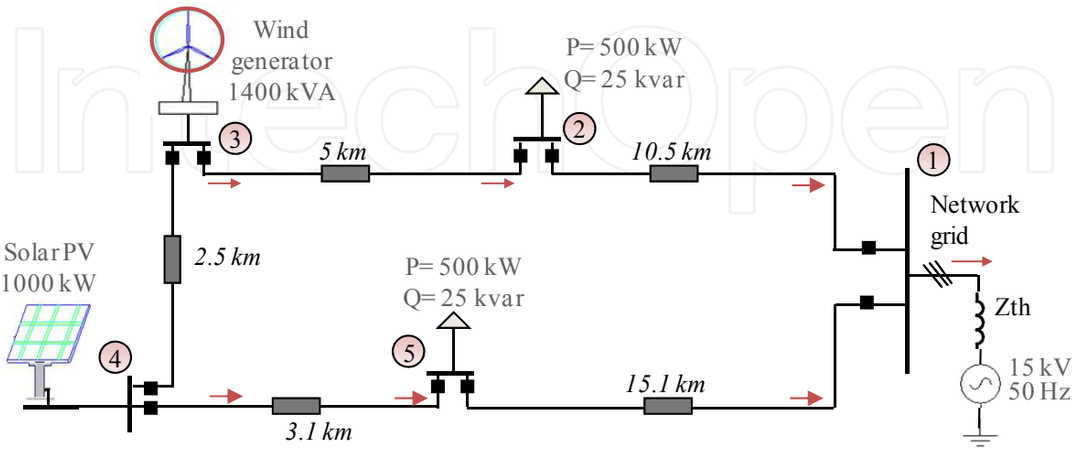

Fig. 12. Distribution network based on capacitive coupling model of wind farms and solar installations.

The electric parameters of the network grid are shown in Table 3.

Element	Parameter	Value
Power grid	Thevenin voltage	15 kV
	Thevenin inductance	17.938 Ω
	Shortcircuit power	12.54 MVA
Underground cable	Positive sequence impedance	0.6969 +*j* 0.492 Ω/km
	Zero sequence impedance	5.945 + *j* 7.738 Ω/km
	Zero sequence susceptance	2.13 μS/km

Table 3. Electric parameters of the network grid.

In node 5, the phase voltage waveform meets the standard regulation of harmonic distortion (THD=5.4%) with a fundamental component of 8.72 kV, as shown in Fig. 13.

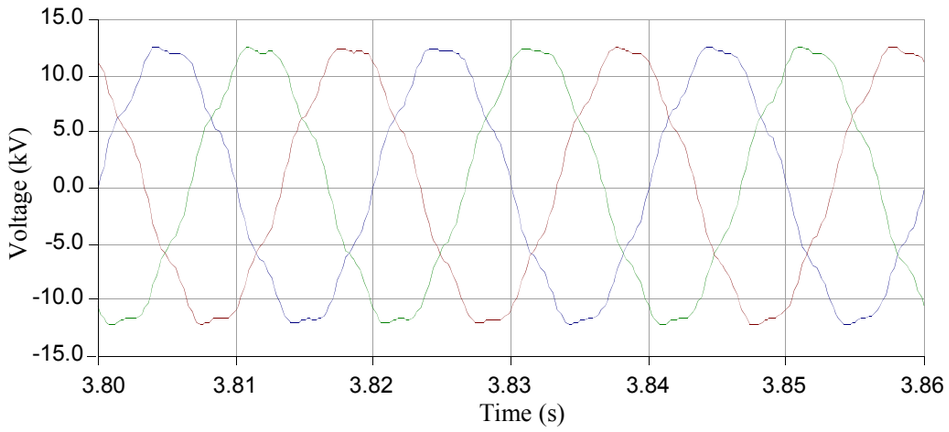

(a)

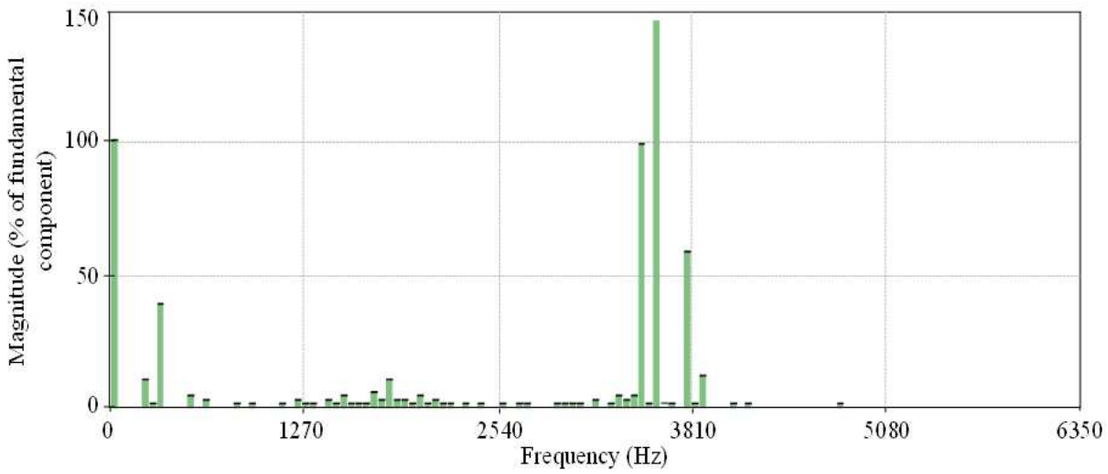

(b)

Fig. 13. Simulation result of the distribution network: (a) phase voltage waveform and (b) FFT analysis of the waveform obtained, at node 5.

Although voltage waveform meets standard regulations, it has been observed an important ground current contribution through the admittance of the underground cables. The ground voltage waveform has a considerable magnitude with peaks reaching 7 V, as shown in Fig. 14. Likewise, the ground current measurement due to the capacitive coupling of these underground cables is also significant as shown in Fig. 15.

The fundamental component of the current waveform is 313 mA, and the THD of this waveform is 190.78%. The most predominant harmonic components are harmonic 72 with 145.22% of the fundamental component, followed by harmonic 70 and 76 with 98.29% and 58.75%, respectively, as shown in Fig. 15a.

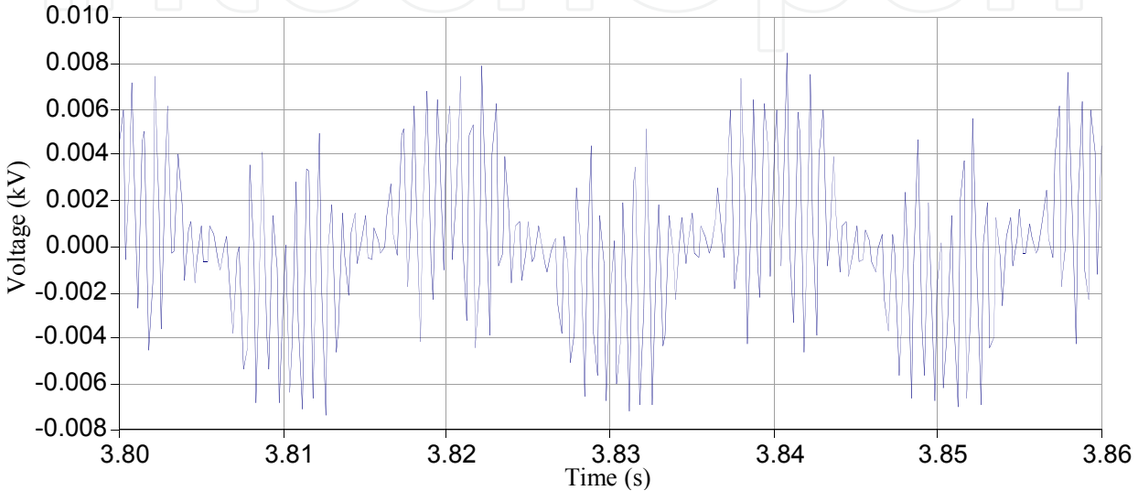

Fig. 14. Simulation result of the distribution network ground voltage waveform at node 5.

These observations point to the importance of controlling the capacitive coupling in load installations connected to networks with DG. Otherwise, end users equipments can be exposed to malfunctioning and lifetime reduction due to the capacitive ground current. Moreover, GPR can reach values of unsafe work conditions.

5. Conclusions

The capacitive coupling models lead to an accurate approximation to the response of distribution network against the frequency spectrum imposed by the switching action of the converters at DG. This approximation is not feasible using simplified models because of the bandwidth limitation for high frequencies.

According to the distribution network under study, a high ground current contribution to grid provided by DG has been detected. Therefore, some preventive actions can be applied to network design stage in order to solve this problem, such as:

- Connection of the PV array to the grounding systems by means of an inductor. The latter element represents high impedance for harmonics current and subsequently reduces the capacitive ground current in the installation.
- Insertion of capacitors between the DC terminals and ground avoids the injection of harmonic current to the PV array, as shown in Fig. 13b, and thereby the noise level and GPR between PV modules and ground is minimized.

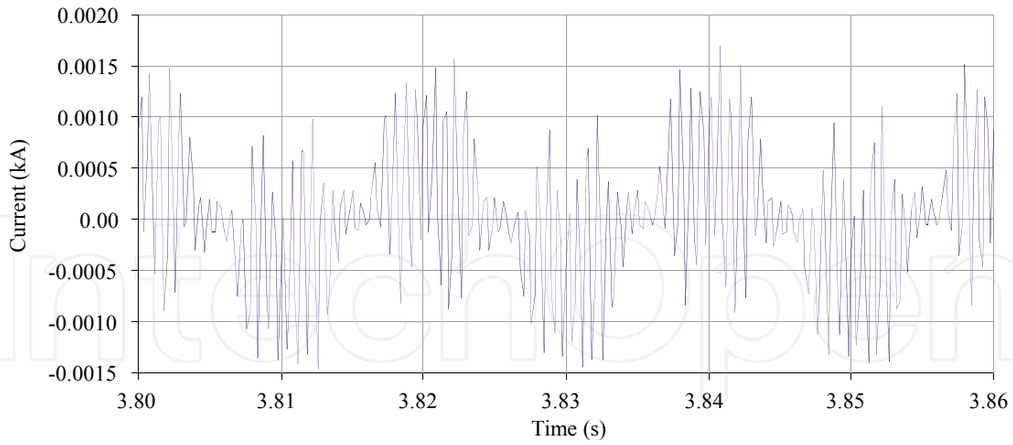

(a)

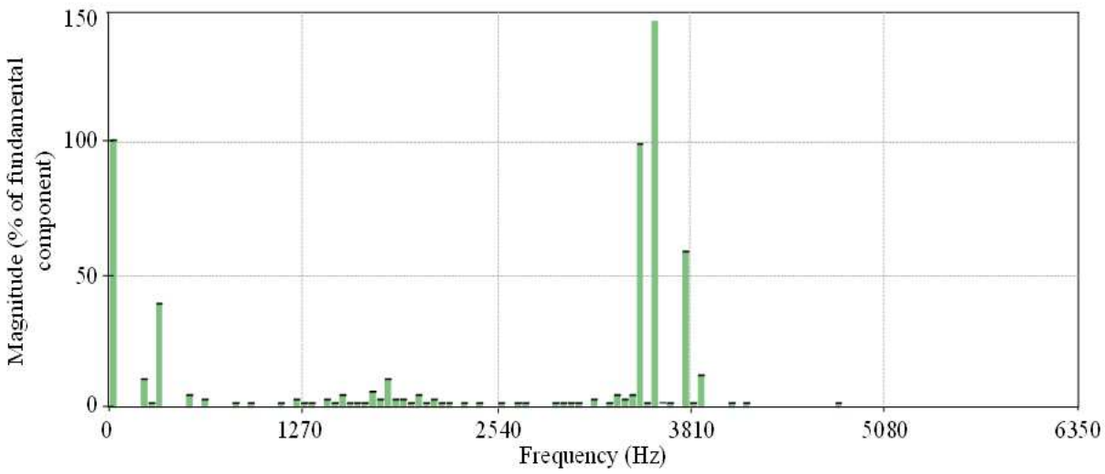

(b)

Fig. 15. Simulation result of the distribution network: (a) current waveform and (b) FFT analysis of the waveform obtained, at node 5.

- Adjustment of the firing pulses frequencies and control strategies to reduce or avoid resonance and capacitive currents by analyzing the ground current with the proposed model.
- Insertion of high-pass filters on the distribution network to avoid end users equipments to be exposed to a high amount of ground current.

6. References

Bellini A., Bifaretti S., Iacovone V. & Cornaro C. (2009). Simplified model of a photovoltaic module, *International Conference on Applied Electronics*, pp. 47–51, ISBN 978-80-7043-781-0, Pilsen, Bohemia, Czech Republic, Sept. 9-10, 2009

Chayawatto N., Kirtikara K., Monyakul V., Jivacate, C. & Chenvidhya D. (2009). DC/AC switching converter modeling of a PV grid-connected system under islanding phenomena, *Renewable Energy,* Vol. 34, No. 12, (2009), pp. 2536–44, ISSN 0960-1481

Chicco G., Schlabbach J. & Spertino F., (2009). Experimental assessment of the waveform distortion in grid-connected photovoltaic installations, *Solar Energy*, Vol. 83, No. 1, pp.1026–39, (2009), ISSN 0038-092X

Comech, M.P., García-Gracia, M., Borroy, S., Villén, M.T. (2010). Protection in Distributed Generation, In: *Distributed Generation*, D. N. Gaonkar, pp. 289-310, In-Teh, ISBN 978-953-307-046-9, Olajnica, Vukovar, Croatia

Conroy, J. & Watson, R. (2009). Aggregate modelling of wind farms containing full-converter wind turbine generators with permanent magnet synchronous machines: transient stability studies, *IET Renewable Power Generation*, Vol. 3, No. 1, (2009), pp. 39–52, ISSN 1752-1424

Dugan, R. C., McGranaghan, M. F., Santoso, S. & Wayne Beaty, H. (2002). *Electrical Power Systems Quality*, McGraw-Hill, (2nd Ed.), ISBN 0-07-138622-X, New York, USA

García-Gracia, M., El Halabi, N., Khodr, H.M. & Sanz, J. F. (2010). Improvement of large scale solar installation model for ground current analysis, *Applied Energy,* Vol. 87, No. 11, (2010), pp. 3467-3474, ISSN 0306-2619

IEC 60479-2 (1987). Effect of current passing through human body. Part II: special aspects. *The International Electrotechnical Commission,* 1987.

IEC Std. 61000-4-7 (2002). Electromagnetic compatibility (EMC). Part 4-7: Testing and measurement techniques. General guide on harmonics and interharmonics measurements and instrumentation for power supply and equipment connected thereto, *International Electrotechnical Commission,* (2002)

IEC Std. 61400-21 (2008), Wind turbines. Part 21: Measurement and assessment of power quality characteristics of grid connected wind turbine, *International Electrotechnical Commission,* (2008).

IEEE Std 519-1992 (1992). (1992). *IEEE recommended practices and requirements for harmonic control in electrical power systems*, Power Engineering Society, 1992

IEEE Std. 80-2000 (2000). *IEEE guide for safety in AC substation grounding*, IEEE Power Engineering Society, 2000

Iliceto A. & Vigotti R. (1998). The largest PV installation in Europe: perspectives of multimegawatt PV, *Renewable Energy,* Vol. 15, No. 1-4, (1998), pp. 48–53, ISSN 0960-1481

Kim S-K., Jeon J-H., Cho C-H., Kim E-S., Ahn J-B. (2009). Modelling and simulation of a grid-connected PV generation system for electromagnetic transient analysis, *Solar Energy*, Vol. 83, No. 5, (2009), pp. 664–78, ISSN 0038-092X

Luna, A., De Araujo, F., Santos, D., Rodriguez, P., Watanabe, E. & Arnaltes, S. (2011). Simplified Modeling of a DFIG for Transient Studies in Wind Power Applications, *IEEE Transactions on Industrial Electronics*, Vol. 58, No. 1, (2011), pp. 9–20, ISSN 0278-0046

Sukamongkol SCY & Ongsakul W. (2002), A simulation model for predicting the performance of a solar photovoltaic system with alternating current loads, *Renewable Energy*, Vol. 27, No. 2, pp. 237–58, (2002), ISSN 0960-1481

Villalva M., Gazoli J, Filho E. (2009), Comprehensive approach to modeling and simulation of photovoltaic arrays, *IEEE Transactions Power Electronics*, Vol. 24, No. 5, pp. 1198–208, (2009), ISSN 0885-8993

Zhou, W., Lou, C., Li, Z., Lu, L., & Yang, H. (2010). Current status of research on optimum sizing of stand-alone hybrid solar-wind power generation systems, *Applied Energy*, Vol. 87, No. 2, pp. 380–389, ISSN 0306-2619

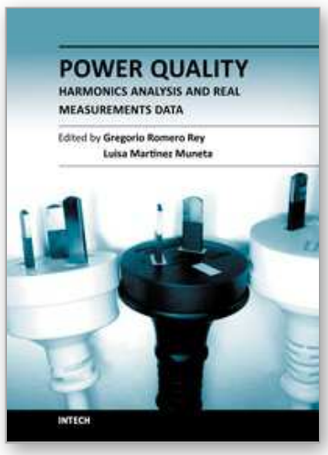

Power Quality Harmonics Analysis and Real Measurements Data
Edited by Prof. Gregorio Romero

ISBN 978-953-307-335-4
Hard cover, 278 pages
Publisher InTech
Published online 23, November, 2011
Published in print edition November, 2011

Nowadays, the increasing use of power electronics equipment origins important distortions. The perfect AC power systems are a pure sinusoidal wave, both voltage and current, but the ever-increasing existence of non-linear loads modify the characteristics of voltage and current from the ideal sinusoidal wave. This deviation from the ideal wave is reflected by the harmonics and, although its effects vary depending on the type of load, it affects the efficiency of an electrical system and can cause considerable damage to the systems and infrastructures. Ensuring optimal power quality after a good design and devices means productivity, efficiency, competitiveness and profitability. Nevertheless, nobody can assure the optimal power quality when there is a good design if the correct testing and working process from the obtained data is not properly assured at every instant; this entails processing the real data correctly. In this book the reader will be introduced to the harmonics analysis from the real measurement data and to the study of different industrial environments and electronic devices.

How to reference
In order to correctly reference this scholarly work, feel free to copy and paste the following:

Miguel García-Gracia, Nabil El Halabi, Adrián Alonso and M.Paz Comech (2011). Harmonic Distortion in Renewable Energy Systems: Capacitive Couplings, Power Quality Harmonics Analysis and Real Measurements Data, Prof. Gregorio Romero (Ed.), ISBN: 978-953-307-335-4, InTech, Available from: http://www.intechopen.com/books/power-quality-harmonics-analysis-and-real-measurements-data/harmonic-distortion-in-renewable-energy-systems-capacitive-couplings

INTECH
open science | open minds

InTech Europe
University Campus STeP Ri
Slavka Krautzeka 83/A
51000 Rijeka, Croatia
Phone: +385 (51) 770 447
Fax: +385 (51) 686 166
www.intechopen.com

InTech China
Unit 405, Office Block, Hotel Equatorial Shanghai
No.65, Yan An Road (West), Shanghai, 200040, China
中国上海市延安西路65号上海国际贵都大饭店办公楼405单元
Phone: +86-21-62489820
Fax: +86-21-62489821

IntechOpen